11th IGTC
Dispatchable technology & innovations for a carbon-neutral society
10-11 October 2023, Brussels, Belgium
Paper ID Number 13-IGTC23

HYDROGEN AND HYDROGEN BLENDED JET AND RECIRCULATION STABILIZED COMBUSTION IN A TURBEC T100 MICRO GAS TURBINE COMBUSTOR

Felix Grimm*, Timo Lingstädt*, Trupti Kathrotia*, Reyhaneh Banihabib**, Mohsen Assadi**, Peter Kutne*, Andreas Huber*

*German Aerospace Center (DLR)
Pfaffenwaldring 38-40
70569 Stuttgart
Germany
felix.grimm@dlr.de

**University of Stavanger (UiS)
Kjell Arholms Gate 41
4021 Stavanger
Norway

ABSTRACT

Hydrogen utilization in decentralized micro gas turbine (MGT) combined heat and power (CHP) systems gains great importance due to the transition towards renewable energy. The work at hand contributes directly to hydrogen usage in CHP by means of experimental and numerical studies. Furthermore, the results are used to improve combustor designs and scale up of the combustion technology.

An existing jet and recirculation stabilized DLR combustor - designed for synthetic gas and partial fuel flexibility - is operated and experimentally investigated with methane hydrogen blends up to pure hydrogen in a Turbec T100 MGT in cooperation with the University of Stavanger (UiS), Norway.

Focal points are emissions behavior and practical usability of the combustion system concerning hydrogen utilization. A wide range of fuel compositions at all significant power levels of the machine are considered. CO and NO_x pollutants are quantified for the combustor emissions behavior. Different dilution air configurations are tested in order to get a picture of equivalence ratio influence for varying fuel compositions. Additionally, experimental results are used as validation data for numerical RANS-based CFD simulations in order to contribute insights for flow field and flame stabilization. CFD results are furthermore used to provide physical explanation for combustor emissions behavior.

Comparison of numerical results with the experiments furthermore focuses on emissions predictions, since no optical access is given in the MGT combustor. It is shown that the applied numerical approaches predict NO_x emissions quantitatively to a certain extent, which is crucial for further combustor design and optimization.

It is demonstrated that the jet and recirculation stabilized combustion system safely and reliably operates with a large range of hydrogen and hydrogen blended fuels over all relevant load points, with at the same time mostly meeting European legal emissions requirements.

NOMENCLATURE

AFN	Air-Fuel Number	-
ATC	Air to Combustion	-
CFD	Computational Fluid Dynamics	-
CHP	Combined Heat and Power	-
DLR	German Aerospace Center	-
EDC	Eddy Dissipation Concept	-
FLOX	Flameless Oxidation	-
FRC	Finite Rate Chemistry	-
MGT	Micro Gas Turbine	-
RANS	Reynolds Averaged Navier Stokes	-
SIMPLE	Semi-Implicit Method for Pressure Linked Equations	-
UiS	University of Stavanger	-
CO	Carbon Monoxide	-
NG	Natural Gas	-
NOx	Nitrogen Oxides	-

INTRODUCTION

Reducing CO_2 emissions is one of the most important influencing factors in reducing the effects of climate change (Masson-Delmotte, et al., 2018; Shukla, et al., 2022). Therefore, the European Commission set the target to reach a climate-neutral economy by 2050 (EuropeanComission, 2021), focusing on a consequent shift to renewable energy sources and clean energy conversion technologies. Due to their fluctuating nature and geographic limitations, solar and wind energy cannot always cover the entire energy demand of all European countries. Therefore, chemical

energy carriers like hydrogen will be necessary to transport and store energy and provide a reliable power and heat supply in a future energy system (IEA, 2019; IEA, 2022) . For example, the European Commission expects to import up to 10 million tons of renewable hydrogen as part of its energy imports (EuropeanComission, 2022).
Because large-scale infrastructure to transport and distribute hydrogen is not available yet, decentralized CHP systems can play an essential role as a first step toward a hydrogen economy. In addition, because of their high overall efficiency and size, only a limited amount of hydrogen is necessary. And they can use green hydrogen close to their production site. Ideally, such systems are fuel flexible to use 100% hydrogen but also mixtures with other fuels if hydrogen is unavailable.
Today, modern gas turbines are limited to H_2 admixtures between 30-60 Vol.-% (ETNGlobal, 2021) when using lean premix combustion without dilution, and MGTs are typically at the lower end of this scale. However, even if MGTs usually operate at a lower pressure (about 3 to 5 bars) than larger gas turbines, and the overall fuel/air ratio is lean due to the low turbine inlet temperatures (about 1000 °C), which can be advantageous for hydrogen combustion, the high combustor inlet temperatures due to recuperation of the exhaust gas heat (up to 650 °C) provide a particular challenge for premixing hydrogen concerning its self-ignition temperature (about 560 °C, atmospheric pressure) and its wide flammable range.
At DLR, new combustion systems are being developed for hydrogen-fuelled energy and aviation applications, based on jet-and recirculation-stabilized combustion. As an intermediate step towards pure hydrogen utilization, several options are conceivable and also pursued, due to urgency and priority. One is to research blends between conventional fuels and hydrogen on novel or established systems. Another is to explicitly benchmark hydrogen capabilities of existing combustion systems.

THE F400S.3 FLOX BURNER

The nomenclature for combustion systems developed at DLR specifies the burner type “F” (for FLOX®, Flameless Oxidation based), followed by the fuel power in kW and the specification of fuel type, for which the burner was designed, in this case “s” (synthetic gas). The subsequent number denotes the development version.
The F400s.3 burner system (Figure 1, (Seliger-Ost, et al., 2020)) was developed for the processing of synthetic gas (design composition 32 Vol.-% H_2, 32 % CO, 18 % CO_2, and 18 %N_2). Full-load operation realizes 360 kW thermal power at an operating pressure of 4 bar. The design point furthermore is at an air-fuel number (AFN) of 2.4 and a pre-heating temperature of 873.15 K.
The F400s.3 is a two-stage burner system, consisting of a jet-and-recirculation stabilized main stage (processing around 90 % of fuel power at design condition) and a swirl-stabilized pilot stage. The pilot stage enhances combustion stability and is used as ignition system. It was previously demonstrated (Bower, et al., 2020) that the burner - as nominally designed - operates reliably and in the range of European emissions requirements in a range of heating values 7 – 49 MJ/kg and an AFN 1.5 – 3.6
The burner system that is investigated in this work is based on - as previously mentioned – the technology of jet-and-recirculation stabilization.

Figure 1: F400s Combustor Module.

The concept is illustrated in Figure 2 (Seliger-Ost, et al., 2020). Air and fuel are injected in the main stage through several nozzles arranged coaxially in circumference. A mixture of air and fuel is to be achieved in a jet-in-co-flow arrangement before issuing into the combustion chamber. A characteristic large inner recirculation zone forms in the combustion chamber due to large axial momentum of the main stage jets. Thus, combustion products are conveyed back into the reaction zone, aiding combustion stability.

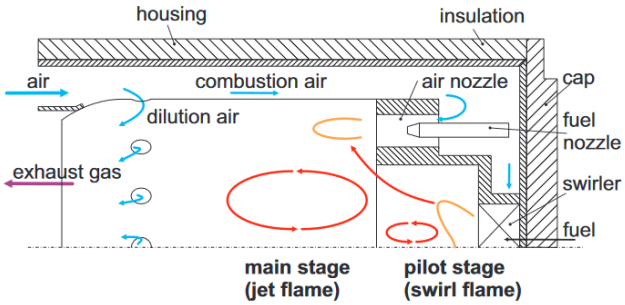

Figure 2: The Jet-and-Recirculation Stabilized Combustion Principle Error! Reference source not found..

The pilot burner forms a separate, compact recirculation zone around the burner main axis and pilot hot gases are transported to the flame root of the main stage nozzles.
Dilution air makes up around two thirds of the overall air fed to the combustion system and it dilutes the combustion exhaust air in a way so it significantly lowers combustor exit temperatures and homogenizes spatial exit temperature distribution.

General results of the burner concept are a homogeneous temperature distribution in the combustion chamber, a wide and stable operation range, and low emissions (Flamme, 2001; Lückerath, et al., 2008). The concept is furthermore promising in avoidance of flashback due to high velocity jets (Lammel, et al., 2011), which is of particular interest for hydrogen combustion.

EXPERIMENTAL SETUP

The test rig is based on a commercial single shaft, recuperated Turbec T100 micro gas turbine (T100PH, Series 2), which is shown in Figure 3. The T100 is equipped with the DLR F400s.3 combustion system. A fuel train has been designed and attached by UiS, in order to be able to realize fuel flexibility and to be able to test methane-hydrogen blends up to 100 % hydrogen.

Figure 3: Turbec T100 with F400s.3 Combustor and Modified Fuel Train.

The MGT can be operated in power generation as well as in co-generation (heat and power) mode. Compressor and turbine of the T100 work with a pressure ratio of around 4.3 and the turbine inlet temperature is in the order of 1225 K. At nominal point (Full-load), the unit is able to provide 100 kW electrical power at 70 krpm with an electrical efficiency of 30 %. Part-load operation is defined at 70 kW electrical power output. Corresponding operational data on the employed T100 and a testing routine depiction can be found in (Banihabib & Mohsen, 2022).
Emissions are measured with a testo 350 analyzer unit. It features a sensitivity of 0.1 – 1 ppm sensitivity for CO and NO_x. For each data point, the measurement period is at least 120 s (targeting 5 min for each measurement point), with value fluctuations in the range of maximum 1 ppm.

MEASUREMENT CAMPAIGN GRID

A range of several operational parameters is tested in the T100 measurement campaign. As previously stated, the current investigation features a benchmark of a DLR combustion system originally developed for synthetic gas processing. Although fuel flexibility for certain types of synthetic gas is given, adaptions are necessary for reliable hydrogen combustion. This applies also for pure methane operation. Since the main focus here is benchmarking towards hydrogen combustion, the main focus is set for higher hydrogen concentrations in the fuel. An extraction from the test matrix, for which results are evaluated in the paper, is drawn in Figure 4.

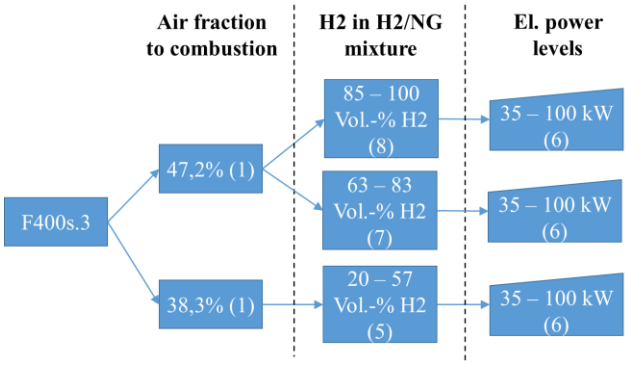

Figure 4: Condensed Matrix of Operation Points from the Measurement Campaign as discussed in the Paper. Number of Data Points in Brackets.

Main adaption for the usage of hydrogen is the application of different cover plates on the dilution air holes, which are located in circumferential alignment in the flame tube after combustion section, as can be seen in Figure 2. Via altered flow resistance, this results in different air fractions available for combustion, denoted by "Air fraction to combustion" in Figure 4. Expectedly, larger amounts of air are used for larger hydrogen concentrations. Subsequently, the fraction of H_2 in the H_2/NG mixture is altered and for each point power levels between 35 – 100 kW are ramped up. Typical air-fuel numbers for two different cover plates are listed in Table 1.

Table 1: Global (Combustor and Mixing Air) and Combustor Air Fuel Number (AFN) Distribution for Several Load Points.

Air frac. Comb. (ATC)	H2 Vol.-%	El. Power	AFN Glob.	AFN Comb.
47.20%	100%	100kW	8.34	3.94
	100%	70kW	9.12	4.30
	67%	100kW	7.36	3.47
	67%	70kW	8.04	3.80
38.30%	14%	100kW	8.06	3.09
	14%	70kW	8.81	3.37
	3%	100kW	7.13	2.73
	3%	70kW	7.79	2.99

Corresponding adiabatic flame temperatures to operation points from Table 1 are displayed in Figure 5, in order to

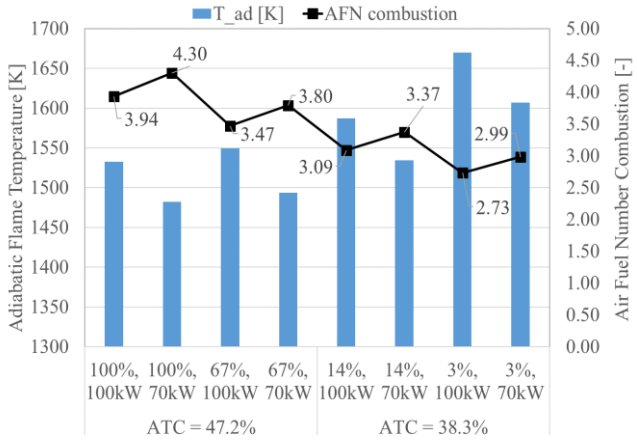

Figure 5: Adiabatic Flame Temperatures and Combustion Air Fuel Numbers according to Table 1.

show orders of magnitudes of expected maximum combustion temperatures.

Naturally, adiabatic flame temperatures follow the trends of local combustion air fuel numbers predominantly. For the measurement campaign at hand they do not significantly differ and are in range of 1480 to 1670K, due to lean combustor operation.

CFD SIMULATION SPECIFICATIONS

Numerical CFD simulations are carried out with the DLR inhouse Code ThetaCOM (Setzwein, et al., 2021), a finite volume based incompressible solver for unstructured grids. Steady state RANS equations are solved with a SIMPLE solution strategy and two-equation k-omega turbulence modeling is performed. Combustion is captured with a novel semi-detailed reaction mechanism for hydrogen and the well-known Finite Rate Chemistry (FRC) approach.

The computational domain is shown in Figure 6. A simplified 60° sector model of the combustor is simulated,

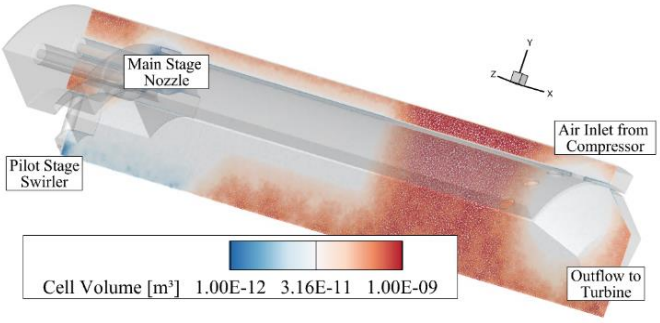

Figure 6: CFD Simplified Computational 60° Model with Combustor Elements and Local Grid Size.

where two main stage nozzles are included in order to capture nozzle-nozzle interaction. The grid consists of 7.7 million points and 44 million elements. It is tetrahedral, with prism layers covering near wall regions. Results are depicted for combustor planes as depicted in Figure 6. Mixing sections and reaction zones are refined with bodies of influences. At inlets, mass flows are specified, whereas the static pressure is defined at the combustor outlet.

Emissions are characterized with averaged combustor exit NO_x concentrations, based on inhouse reaction mechanism DLR Concise that contains emissions pathways (Kathrotia, et al., 2021). A customized reduced mechanism is used in this work. Results are validated with experimental findings. Subsequently, the CFD results provide additional information to experimental data on flow field, reaction zones, and temperature distribution.

Results from four operation points are explicitly analyzed in the paper. Simulated conditions are listed in Table 1 for ATC = 47.2%. Thus, only the configuration adapted for hydrogen usage are simulated and evaluated with CFD, covering a full-load and part-load case for two different H_2 fractions (100 Vol.-% and 68 Vol.-%), respectively.

RESULTS AND DISCUSSION

At first, results of emissions measurements are shown. Consequently, CFD results for emissions modeling are opposed to experimental findings and finally, the analysis is complemented by CFD results for flow field and combustion. Emissions results are structured three-fold, oriented at the structure of the measurement campaign with respect to hydrogen content in the fuel, as indicated in Figure 4.

At first, most H_2 relevant combustor configuration (ATC = 47.2 %) results are shown for larger and medium hydrogen fractions in the fuel, followed by the NG-favoring configuration (ATC = 38.3 %) results.

Due to the lack of legal emissions limits definition for hydrogen combustion, results are compared with TA Luft (TALuft, 2002) limits for mixtures and natural gas.

NO_x and CO Emissions for Large Hydrogen Fractions and ATC = 47.2 %

Measured NO_x and CO emissions for ATC = 47.2 % and large hydrogen fractions are displayed in Figure 7 and Figure 8.

Expectedly, NO_x emissions rise with increasing power, due to larger fuel power entry, resulting in larger peak temperatures. NO_x remains below 70 ppm for the investigated range, peaking in 97 – 100 % hydrogen usage. Larger fractions of hydrogen consistently result in higher NO_x production. The main cause for this is increased adiabatic flame temperature, the larger the hydrogen fractions are.

For inconsistencies in the measurements for large hydrogen fractions and high electrical powers, hysteresis effects due to difficulties in experimental procedures are held responsible. Due to fuel supply with hydrogen bundles and

a very large demand of hydrogen volume flux, certain ramping procedures of the gas turbine had to be accepted, leading to inaccurate emission results.
CO emissions are below existing legal limits for large hydrogen fractions almost consistently for all power levels investigated.

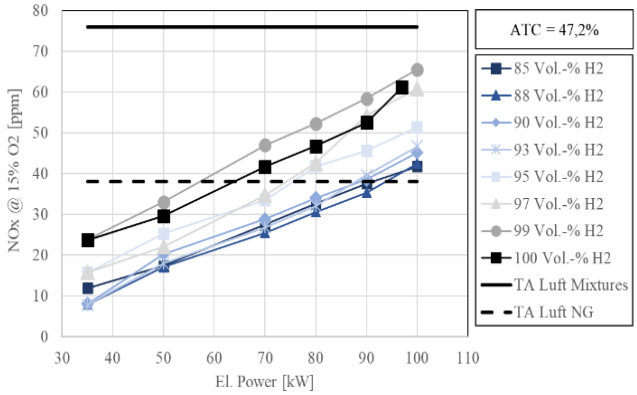

Figure 7: NOx Emissions of F400s.3 for larger fractions of Hydrogen, Air to Combustion (ATC) at 47.2 %.

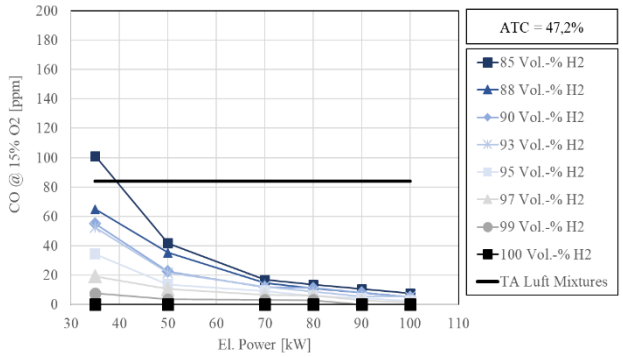

Figure 8: CO Emissions of F400s.3 for larger fractions of Hydrogen, Air to Combustion (ATC) at 47.2 %.

The lower the hydrogen fraction in the fuel, the larger the amount of CO emissions. This is consistent with previous observations (Bower, et al., 2020), where the F400s.3 combustor tends to produce larger CO the more the fuel composition is shifted to higher methane fractions. Furthermore, air-fuel numbers are significantly larger towards part-load, thus fostering higher CO emissions.

NO_x and CO Emissions for Medium Hydrogen Fractions and ATC = 47.2 %

NO_x emissions for medium hydrogen volume fractions are shown in Figure 9. They show a consistent situation with NO_x emissions for larger hydrogen fractions (Figure 7). In general, levels rise for increasing power levels of the gas turbine and larger hydrogen volume fractions result in higher NO_x values, again due to higher adiabatic flame temperatures. Naturally, NO_x values are lower compared to large hydrogen fractions (Figure 7) due to comparably lower flame temperatures.

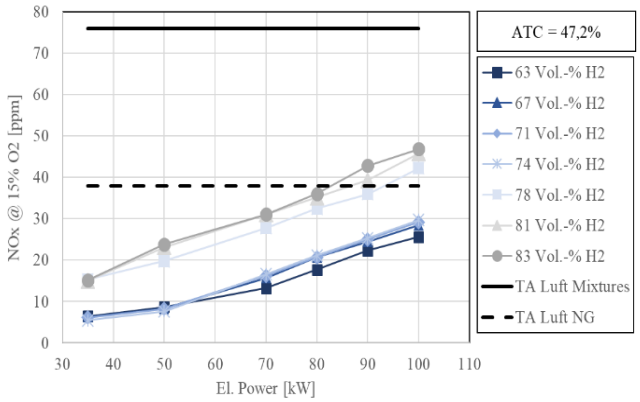

Figure 9: NO_x Emissions of F400s.3 for Medium Fractions of Hydrogen, Air to Combustion (ATC) at 47.2 %.

CO emissions for medium hydrogen volume fractions are analyzed with Figure 10. Once again, trends are consistent with CO emissions for high hydrogen fractions (Figure 8).

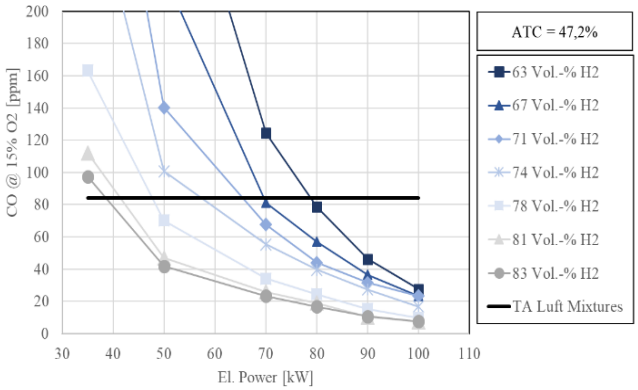

Figure 10: CO Emissions of F400s.3 for Medium Fractions of Hydrogen, Air to Combustion (ATC) at 47.2 %.

A significant difference are larger absolute values far beyond 200 ppm for lowest power levels and a much sooner increase with decreasing power. This is in line with the combustor behaving more in the less-optimized natural gas operation range. Another possible factor is a larger flame lift-off, lower air-fuel mixing quality and the reaction zone being subject to higher turbulent fluctuation farther downstream in the combustor.

NO_x and CO Emissions for Smaller Hydrogen Fractions and ATC = 38.3 %

NO_x values for lowest hydrogen fractions generally show larger levels compared to medium hydrogen fractions

in the fuel (Figure 9). At first glance, this appears counter-intuitive.

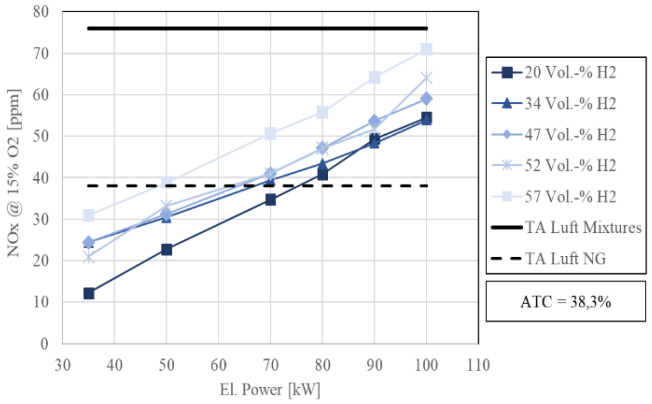

Figure 12: NO_x Emissions of F400s.3 for Smaller Fractions of Hydrogen, Air to Combustion (ATC) at 38,3 %

However, different aspects for combustor configuration and operation come into play, which have to be taken into consideration. A major difference is the employment of a different cover plate for mixing air (as discussed previously, see Figure 2, Figure 4, and Table 1). Less air is led to combustion for large natural gas fractions (ATC = 38.3 %) and this leads to lower air fuel numbers (Table 1), increasing combustion temperatures and NO_x values.
Furthermore, a different pilot mapping and different power splits between main and pilot stage of the burner system have to be applied, in order to ensure stable combustion for natural gas operation. For natural gas, this means applying more power for the pilot, which is known for increasing NO_x levels due to a hotter pilot combustion regime.

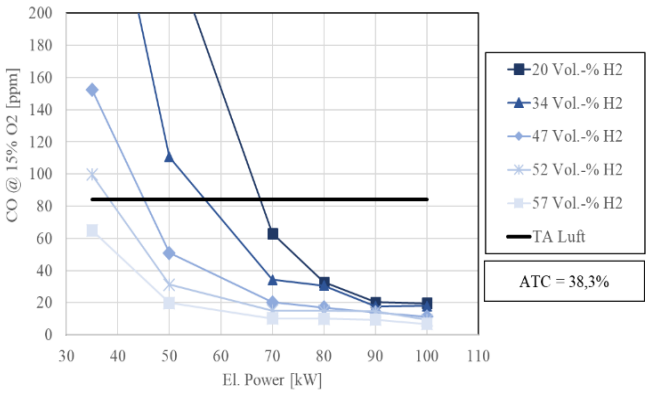

Figure 11: CO Emissions of F400s.3 for Smaller Fractions of Hydrogen, Air to Combustion (ATC) at 38,3 %.

Those points naturally apply for CO emissions measurements for low hydrogen fractions also, as shown in Figure 12. Compared to medium hydrogen fractions, CO levels are lower and increase later with decreasing power. Larger methane contents in the fuel foster higher CO levels. On the contrary however, combustion is generally more stabilized by increased pilot power and air fuel numbers are consistently lower for ATC = 38.3 % (Table 1). Therefore, CO levels are lower compared to medium hydrogen fractions and operational range widens.
Emissions of the studied combustion system are summarized in Figure 14. The heat map features dark colors for larger emission values. By the division into different combustor configurations (different ATC), it becomes evidently visible that increased air to combustion is crucial for larger hydrogen fractions in the fuel. This point has to be further addressed for hydrogen specific combustor development. The color shading in Figure 14 also indicates that carried out measurements are highly consistent; thermal NOx emissions increase for larger hydrogen fractions and higher electrical power, whereas the opposite effect is present for CO emissions.

Comparison of Experimental and Numerical NO_x Emissions Results

Emissions between experimental and numerical results are compared by four discrete data points for CFD and corresponding load development from T100 measurements. Results are displayed in Figure 13.
The shown study focuses on NOx, since CO emissions are strongly dependent on unsteady effects and turbulence-chemistry interaction, which cannot be depicted with steady state RANS CFD. Furthermore, the study aims at establishing and investigating hydrogen combustion, where CO emissions play a subordinate role.

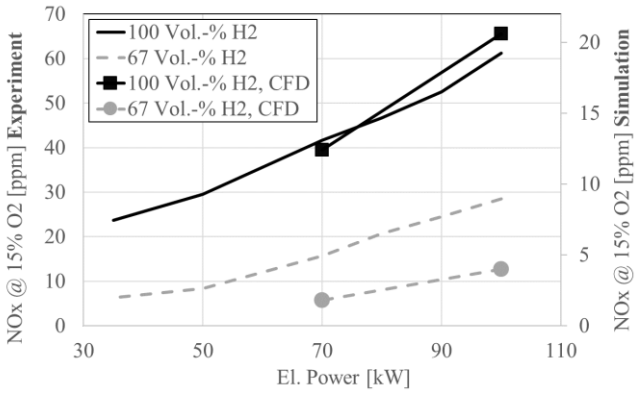

Figure 13: Comparison of NO_x Emissions from Measurements (Left Axis) and Numerical Simulation (Right Axis).

To be able to evaluate NO_x emission prediction capabilities in the CFD approach, experimental and numerical results are depicted on different vertical axes. In that way, true slopes of emission curves are shown.

It is found that slopes of NO_x emission curves are properly reproduced by the CFD approach. Therefore, NO_x trends from CFD are capable of serving as a parameter in combustor development, especially for hydrogen-optimized combustion systems as currently in design.
Besides NO_x trends, there are discrepancies between experiment and simulation. Numerical results consistently underpredict measured values. However, absolute values are in the same order of magnitude (e.g. 61 ppm (Exp, 100 % H_2) vs. 20.6 ppm (Sim, 100 % H_2)). This is highly remarkable due to the employment of a RANS approach with a relatively compact reaction scheme.
The robust and computationally efficient CFD approach that is used here for NO_x reproduction and flow field description is therefore rated as highly suitable for being applied in hydrogen-fueled combustor development.
Considering this level of accuracy in reproducing experimental findings, additional data on flow field and combustion is added and discussed.

CFD Results

Contour results are displayed (Figure 15) on axial planes through the numerical model, incorporating a main stage nozzle, a mixing orifice, and the pilot stage swirler in part.
Axial velocity fields show typical jet-and-recirculation stabilized burner flow field characteristics. Since cases with increased air through combustion are viewed (ATC = 47.2 %), jet velocities are comparably high, in the order of magnitude of 150 m/s. Due to limited combustion chamber space, this leads to a pronounced inner recirculation zone. In the presented cases, recirculation zones of pilot and main system are interconnected. The pilot system shows a characteristic swirled flow field with spatial expansion in axial direction.
The main stage jets furthermore seem to produce large scale turbulent fluctuation, due to their pronounced issuing into the combustion chamber with high momentum.
Heat release profiles in Figure 15 show interesting common features throughout the load cases but also distinct differences. Pilot reaction zone position appears to be stable in terms of extension and shape throughout the investigated operation conditions, almost regardless of hydrogen content or gas turbine load.
A different scenario is at display for the main stage. Especially for hydrogen only, reaction zones are located farther upstream, close to the jet orifice. A rather small difference in fuel flow rate at part load conditions does however result in visible impacts for flame lift-off.

Cases with large methane fuel contents show an elongated reaction zone in main flow direction. It appears that the reaction zone is subject to local quenching in near wall regions. This observation is in line with increasing CO emissions for lower hydrogen contents in fuel.
Temperatures in Figure 15 are widely homogeneous, as is expected and desired in jet and recirculation stabilized combustion. Upstream temperature peaks are observed for large hydrogen fuel concentrations, which is a consequence from the very compact reaction zone. Main stage temperature spots are however quickly dissipated into the combustion chamber. Significant large temperature spots are prevailing for all investigated cases in the swirl stabilized pilot stage which is critical for NO_x production and in the long-term posts negative impact for the combustor structures in the pilot regions.

NOx [ppm]		Vol.-% H2																			
		20	34	47	52	57	63	67	71	74	78	81	83	85	88	90	93	95	97	99
El. Power [kW]	35	12.21	24.41	24.41	20.91	30.89	6.43	6.28	6.12	5.44	15.30	15.05	15.15	11.90	7.93	8.08	7.86	15.64	15.84	23.80
	50	22.72	30.44	31.17	33.15	38.82	8.71	8.33	8.24	7.63	19.83	23.17	23.80	17.37	17.05	20.26	17.95	25.30	22.05	33.06
	70	34.73	39.42	41.02	41.02	50.64	13.22	15.69	16.23	16.60	27.77	31.04	31.06	27.50	25.50	28.86	26.85	33.47	34.74	46.97
	80	40.83	43.44	47.11	47.10	55.78	17.72	20.70	20.70	21.16	32.45	35.16	36.04	32.60	30.58	34.00	32.08	41.74	42.59	52.25
	90	49.40	48.36	53.67	51.73	64.26	22.34	24.53	25.01	25.29	35.95	39.32	42.84	37.55	35.38	38.58	39.57	45.53	54.24	58.37
	100	54.49	53.89	59.05	64.08	70.94	25.63	28.47	29.17	29.75	42.26	45.86	46.84	41.78	42.50	45.21	46.69	51.39	60.83	65.53
		ATC = 38.3%					ATC = 47.2%														

CO [ppm]		Vol.-% H2																			
		20	34	47	52	57	63	67	71	74	78	81	83	85	88	90	93	95	97	99
El. Power [kW]	35	717	336	153	99.7	65	740	562	408	289	163	112	97.4	101	64.9	55.1	52.4	34.3	19.3	7.68
	50	243	111	51	31.2	19.8	334	223	140	101	70.2	47	41.8	41.8	35.4	22.5	21.6	13.7	10.5	3.48
	70	63.1	34.3	20.3	15.2	10.1	124	81.1	67.6	55.3	34	25.9	23.2	16.8	14.7	11.9	12.2	9.3	6.43	3.13
	80	32.7	30.7	17	14.9	9.92	78.5	56.9	44	39.7	24.3	18.9	16.8	13.6	11.1	11.3	8.75	5.92	6.04	3.02
	90	20.2	17.8	14	14.6	9.52	46.1	36.4	31.6	27.3	15.2	10.3	10.6	10.6	8.04	8.15	5.53	4.19	2.77	0
	100	19.6	18	11.4	9.15	6.87	27.5	23.3	23.3	16.7	9.71	7.44	7.6	7.6	5.15	5.2	5.34	2.7	1.33	0
		ATC = 38.3%					ATC = 47.2%														

Figure 14: Matrix of NOx and CO Emissions in ppm @15% O2.

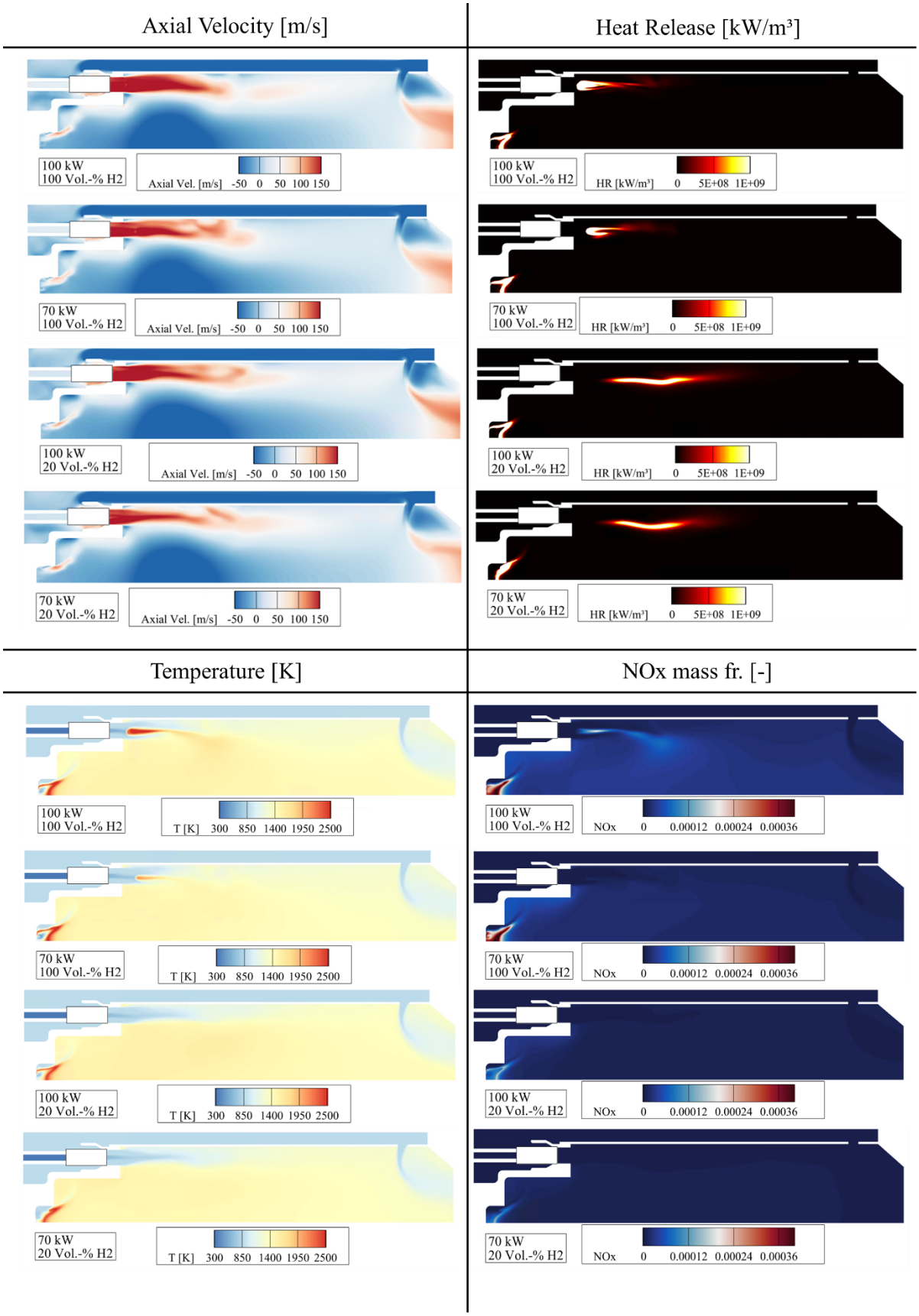

Figure 15: CFD Contour Plot Results for Axial Velocities, Heat Release, Temperatures and NO_x mass fractions.

As the CFD results in Figure 15 demonstrate, NO_x is produced mainly in the pilot stage, where temperature hot spots are prevailing. It is therefore concluded that thermal NO_x is the main mechanism for pollutant formation.
Significant modifications of the burner system regarding optimization for pollutant emissions are therefore clearly the employment of an either alternative or highly optimized pilot stage for NO_x and the modification of main stage nozzle position for lowering CO emissions.

CONCLUSIONS

In this work, hydrogen and hydrogen/NG mixtures were used as fuels into a 400 kW DLR combustion system based on jet and recirculation stabilized burner technology, originally developed and optimized for synthetic gas usage. Operation was carried out in a Turbec T100 gas turbine at UiS.
The study was carried out to gain knowledge of hydrogen combustion, benchmark an existing combustor under realistic operation conditions, and to strengthen CFD combustor design tools for hydrogen applications. Only small but global modifications (fractions of mixing and combustion air) were applied.
It was found that the DLR burner system F400s.3 was able to reliably handle the tested fuels, ranging from 20/80 to 100/0 (Vol.-% H_2 / Vol.-% NG) gas compositions. In all cases, stable operation was achieved. The burner system however showed relatively high NO_x levels towards higher load conditions and the main contribution was traced back to thermal NO_x emerging in the pilot sub-system. High CO levels were observed mainly for lower hydrogen fuel fractions and lower load points of the T100 gas turbine. CO emissions were by default satisfactory for largest hydrogen contents. Overall, it can be stated that the burner system is able to handle hydrogen fuels within existing legal emissions limits, as far as mixing air cover plates are used in order to adapt combustion regimes.
It was furthermore shown that the applied CFD combustor design tools are highly feasible for hydrogen burner design. NO_x values were reliably predicted in terms of trends as well as order of magnitude values. The detailed CFD results furthermore revealed a highly consistent physical description of the burner system, as indicated by experimental emission trends. The employed CFD RANS tool is explicitly robust and computationally cheap compared to field testing.
As a major outcome of this study, it was demonstrated that the DLR jet and recirculation stabilized burner technology is already capable of handling hydrogen to a certain extent, but very tangible modifications for hydrogen-optimized burners are possible and already being derived. Based on the studied F400 burner system, several developments for hydrogen optimized burners of different size classes are on the way.
Besides heading for the keyword retrofit in the context of applying different fuel types to an MGT in this work, the DLR burners based on jet- and recirculation stabilized combustion have considerable potential for up- and downscaling, which is founded in the design principles of the concept. Downscaling of the combustion concept for small MGTs like the MTT EnerTwin (about 3 kW electrical power) was already demonstrated (Seliger-Ost, et al., 2020), and DLR recently developed an F1000 combustor for the Aurelia A400 gas turbine (400 kW electrical power).
Because of the similar boundary conditions and functional principles for the combustion system, a hydrogen-optimized or fuel-flexible combustor is expected to be scaled and readily retrofitted into existing industrial gas turbines with can-annular combustors, too. Of course, such a retrofit would involve further adaptation of the gas turbine (e.g., fuel path, control system), and there might be limitations for specific gas turbine models. But such a combustion system might open up a pathway to extend the lifetime of existing systems and allow for a fast transition to hydrogen.

REFERENCES

Banihabib, R. & Mohsen, A., 2022. A Hydrogen-Fueled Micro Gas Turbine Unit for Carbon-Free Heat and Power Generation. *Sustainability*, 14(20), p. 13305.

Bower, H. et al., 2020. Experimental Analysis of a Micro Gas Turbine Combustor Optimized for Flexible Operation with Various Gaseous Fuel Compositions. *J. Eng. Gas Turbines Power*, 142(3), p. 031015.

ETNGlobal, 2021. Hydrogen Gas Turbines - The Path Towards A Zero-Carbon Gas Turbine.

EuropeanComission, 2021. Comm. Del. Reg. (EU) 2022/1214 of 9 March 2022 amending Del. Reg. (EU) 2021/2139 as regards economic activities in certain energy sectors and Delegated Regulation (EU) 2021/2178 as regards specific public disclosures for those economic activities. *Official Journal*, pp. 1-45, L188.

EuropeanComission, 2022. Communication from the commission to the European Parliament, the European council, the council, the European economic and social committee and the committee of the regions REPowerEU plan. COM/2022/230 final. *European Commission Communication*.

Flamme, M., 2001. Low NOx Combustion Technologies for High Temperature Applications. *Energy Convers. Manag.*, 42(15), p. 1919–1935.

IEA, 2019. The Future of Hydrogen. *International Energy Agency*.

IEA, 2022. Global Hydrogen Review. *International Energy Agency*.

Kathrotia, T. et al., 2021. Combustion kinetics of alternative jet fuels, Part-II: Reaction model for fuel surrogate. *Fuel*, Volume 302, p. 120736.

Lammel, O. et al., 2011. Experimental Analysis of Confined Jet Flames by Laser Measurement Techniques. *J. Eng. Gas Turbines Power*, 134(4), p. 041506.

Lückerath, R., Meier, W. & Aigner, M., 2008. FLOX Combustion at High Pressure with Different Fuel

Compositions. *J. Eng. Gas Turbines Power*, 130(1), p. 011505.
Masson-Delmotte, V. et al., 2018. Global Warming of 1.5°C.An IPCC Special Report on the impacts of global warming of 1.5°C above pre-industrial levels and related global greenhouse gas emission pathways, (...). *Cambridge University Press*.
Seliger-Ost, H., Kutne, P., Zanger, J. & Aigner, M., 2020. Experimental Investigation of the Impact of Biogas on a 3 kW Micro Gas Turbine FLOX®-Based Combustor. *J. Eng. Gas Turbines Power*, 143(8), p. 081020.
Setzwein, F., Ess, P. & Gerlinger, P., 2021. An implicit high-order k-exact finite-volume approach on vertex-centered unstructured grids for incompressible flows. *Journal of Computational Physics*, p. 110629.
Shukla, P. et al., 2022. Climate Change 2022: Mitigation of Climate Change. Contribution of Working Group III to the Sixth Assessment Report of the Intergovernmental Panel on Climate Change. *Cambridge University Press*.
TALuft, 2002. First General Administrative Regulation Pertaining the Federal Immission Control Act (Technical Instructions on Air Quality Control - TA Luft). *Federal Ministry for Environment, Nature Conservation and Nuclear Safety*.
Zornek, T., Monz, T. & Aigner, M., 2015. Performance analysis of the micro gas turbine Turbec T100 with a new FLOX-combustion system for low calorific fuels. *Applied Energy*, Volume 159, pp. 276-284.

ATTACHMENT

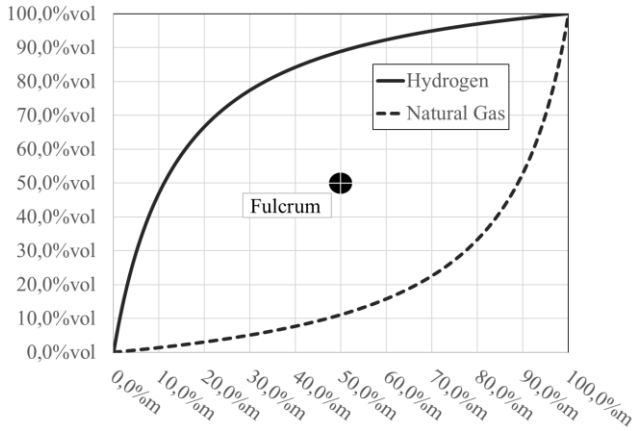

Figure 16: Relation for Volume and Mass Fraction for an Ideal Gas Hydrogen – Natural Gas Mixture.